BIOCHEMISTRY
including biophysical chemistry & molecular biology

Article

pubs.acs.org/biochemistry

# The Internal Dynamics of Mini c TAR DNA Probed by Electron Paramagnetic Resonance of Nitroxide Spin-Labels at the Lower Stem, the Loop, and the Bulge

Yan Sun,[†] Ziwei Zhang,[‡,∥] Vladimir M. Grigoryants,[†] William K. Myers,[†,⊥] Fei Liu,[†] Keith A. Earle,[§] Jack H. Freed,[‡] and Charles P. Scholes*[,†]

[†]Department of Chemistry, University at Albany, 1400 Washington Avenue, Albany, New York 12222, United States

[‡]Department of Chemistry and Chemical Biology and ACERT, Cornell University, Ithaca, New York 14853, United States

[§]Department of Physics, University at Albany, 1400 Washington Avenue, Albany, New York 12222, United States

Supporting Information

**ABSTRACT:** Electron paramagnetic resonance (EPR) at 236.6 and 9.5 GHz probed the tumbling of nitroxide spin probes in the lower stem, in the upper loop, and near the bulge of mini c TAR DNA. High-frequency 236.6 GHz EPR, not previously applied to spin-labeled oligonucleotides, was notably sensitive to fast, anisotropic, hindered local rotational motion of the spin probe, occurring approximately about the NO nitroxide axis. Labels attached to the 2′-aminocytidine sugar in the mini c TAR DNA showed such anisotropic motion, which was faster in the lower stem, a region previously thought to be partially melted. More flexible labels attached to phosphorothioates at the end of the lower stem tumbled isotropically in mini c TAR DNA, mini TAR RNA, and $\psi_3$ RNA, but at 5 °C, the motion became more anisotropic for the labeled RNAs, implying more order within the RNA lower stems. As observed by 9.5 GHz EPR, the slowing of nanosecond motions of large segments of the oligonucleotide was enhanced by increasing the ratio of the nucleocapsid protein NCp7 to mini c TAR DNA from 0 to 2. The slowing was most significant at labels in the loop and near the bulge. At a 4:1 ratio of NCp7 to mini c TAR DNA, all labels reported tumbling times of >5 ns, indicating a condensation of NCp7 and TAR DNA. At the 4:1 ratio, pulse dipolar EPR spectroscopy of bilabels attached near the 3′ and 5′ termini showed evidence of an NCp7-induced increase in the 3′−5′ end-to-end distance distribution and a partially melted stem.

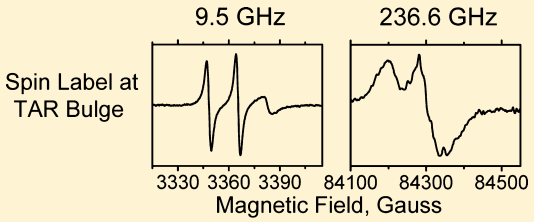


The purpose of this study is to understand the internal dynamics of a model stem−loop oligonucleotide from HIV-1 and the change in these dynamics upon its interaction with HIV-1 nucleocapsid protein NCp7. The stem−loop structure is found in the TAR (transactivation response) region of c TAR DNA and TAR RNA. As shown both in vivo[1,2] and in vitro,[3,4] the binding of NCp7 inhibits self-priming within such a stem−loop structure and promotes annealing for the formation of duplexes between complementary TAR RNA and TAR DNA. In vitro annealing has been conducted in quantitative kinetic detail[3,4] using "mini c TAR DNA" (Figure 1A). As we have previously shown with the simpler $\psi_3$ RNA stem−loop structure,[5] stem−loop oligonucleotide complexes with NCp7 undergo structural rearrangements, whose dynamics are amenable to EPR spin-label methods. NCp7 (Figure 1B) is adapted for specific binding to a diversity of oligonucleotides in base-unpaired regions by hydrophobic and hydrogen bonding, and electrostatic interactions between cationic NCp7 and anionic oligonucleotides enhance both specific and nonspecific binding.

Mini c TAR DNA (Figure 1A) has an apical loop and an internal bulge, both containing unpaired bases and potential centers for dynamic structural modulation and NCp7 binding. Imino hydrogen exchange has provided evidence of an intrinsically destabilized double-strand region below the bulge.[6] Nuclear magnetic resonance (NMR) techniques that resolve residual dipolar couplings have pointed to the internal bulge of TAR RNA as a locus for large bending motions and for exchange between conformations adapted to the recognition of small molecule inhibitors and TAR binding proteins like NCp7 and TAT.[7−10] NMR structures of mini c TAR DNA are likewise consistent with several coexisting conformations,[6,11] and the TAR DNA structure, as opposed to the TAR RNA structure, is a less stable, more dynamic structure and is more open to NCp7 perturbation.

In our previous EPR work, only the 5′ terminus of the $\psi_3$ RNA stem was labeled.[5] In contrast, we now extend our study to a comparison of dynamic EPR signatures in the stem (SLA, SLB, and SL2), loop (SL1), and bulge (SL3) of the more complex TAR, and we additionally use high-sensitivity, high-field EPR for this purpose.[12] A previous spin-label study of oligonucleotides used only low-field 0.35 T, 9.5 GHz X-band EPR to monitor site-specific spin probes.[13−20] High-field, high-frequency 8.4 T, 236.6 GHz EPR[12,21−24] is now a mature

**Received:** August 5, 2012
**Revised:** September 21, 2012
**Published:** September 25, 2012

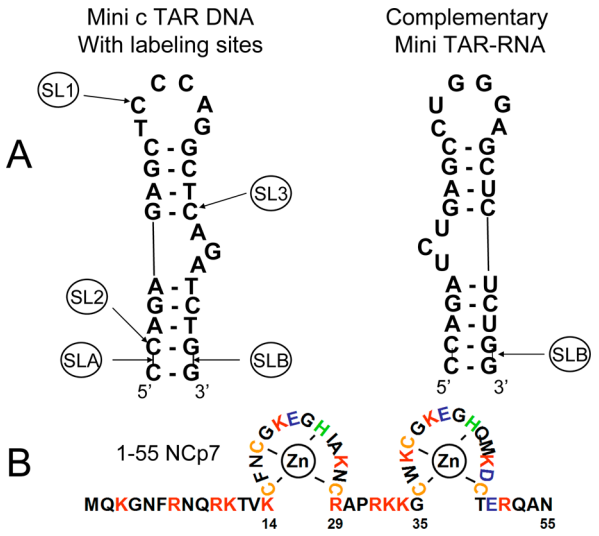


**Figure 1.** (A) Secondary structure of mini c TAR DNA and mini TAR RNA and the position of spin-labels used in this study primarily of mini c TAR DNA. (B) Primary structure of 1−55 NCp7.

technique that is sufficiently sensitive that it provides spectra from ∼100 $\mu$M solutions of oligonucleotides in aqueous solution. High-frequency, high-field EPR provides much better definition of the fast (subnanosecond) components of probe motion because the high field markedly increases the importance of the nitroxide **g** tensor in determining spectral line shape. The slowly relaxing local structure (SRLS) model[12,25−27] has become available for fitting spin-label spectra that result from fast internal motion of a spin-label restrained on a more slowly tumbling macromolecule, and it can be used to reduce spectral ambiguity by simultaneous analysis of spectra at, e.g., 236.6 and 9.5 GHz. Through a combination of 236.6 and 9.5 GHz EPR, supplemented by spectra from intermediate frequencies in the future, one will even more readily be able to spectroscopically separate the global tumbling and large-scale nanosecond bending motions from fast internal subnanosecond fluctuations at the probe.[27]

The spin-label attached at the 5′ terminus of $\psi_3$ RNA through a thio−amido linkage[5] had its tumbling as reported in prior 9.5 GHz experiments progressively impeded by added NCp. In this work, we have extended spin-label monitoring sites to the stem, loop, and bulge structures of mini c TAR DNA using less mobile ureido−2′-amino linkages at SL2, SL1, and SL3, respectively, and for the 3′ and 5′ ends, using the thio−amido linkages as described previously with $\psi_3$ RNA. Loop, bulge, and destabilized stem regions have all been proposed and frequently found to be specific targets for NCp7 in its interaction with TAR RNA and TAR DNA stem−loop oligonucleotides,[7−10,28−30] and thus, we monitor them. A recent NMR-monitored study of mini c TAR DNA bound to 11−55 NCp7 (which lacks the highly basic, cationic tail of residues 1−10 of 1−55 NCp7) showed tryptophan intercalation and hydrogen bonding to unpaired bases in the lower stem below the bulge, but that study also reported gel retardation evidence for another weaker binding elsewhere.[11] Although a previous 9.5 GHz EPR study by Sigurdsson and coworkers, using a form of TAR RNA lacking the apical loop, reported perturbation to the label EPR signal from binding of TAR inhibitors and peptides, there was no study of the interaction of TAR forms with NCp7.[14−16,18]

At low ionic strengths when the ratio of NCp7 to $\psi_3$ RNA bases was 6−7, a marked decrease in the rate of probe tumbling occurred.[5] Such a decrease indicated large, slowly tumbling $\psi_3$ RNA−NCp7 complexes. The decreased rate of probe tumbling depended not only on ionic strength-dependent electrostatic attraction between cationic NCp7 and anionic RNA but also on the presence of intact Zn fingers of NCp7. Motivated by the in vitro annealing of mini c DNA and mini TAR RNA,[3,31] we follow now the change in dynamics of our mini c TAR DNA at a coverage of approximately six to seven bases per NCp7. At a coverage of six to seven bases per NCp7, NCp7 performs as a chaperoning agent that will recognize secondary structures within individual nucleotide strands, destabilize these secondary structures, and enhance subsequent annealing of complementary oligonucleotides into duplexes.

Previous fluorescence resonance energy transfer (FRET) studies have provided evidence of the existence of destabilized secondary structure in the c TAR DNA when it is covered with NCp7.[32−34] Here pulse dipolar spectroscopy (PDS) is used to probe the distances and distance distributions between bilabels connected to 3′ (SLB) and 5′ (SLA) ends of mini c TAR DNA at a coverage of approximately six to seven bases per NCp7 as a monitor of the unwinding and destabilization of the stem structure. Because of the smaller nitroxide probes, their shorter tethers, and mathematically reliable method for extracting pair distributions,[35,36] the pulsed EPR technique provides not only precise distances (whereas FRET provides distance estimates) but also explicit quantitative information about the distribution of end-to-end distances in NCp7-destabilized mini c TAR DNA. This study is thus primarily a dynamic study, but pulse dipolar spectroscopy yields relevant structural information about the destabilization of the DNA double strand within the NCp7-destabilized c TAR DNA structure.

## MATERIALS AND METHODS

**Preparation and Characterization of Spin-Labeled Mini c TAR Derivatives.** Spin-labels were attached at positions SLA, SLB, SL1, SL2, and SL3 shown in Figure 2.

The thio-amido phosphorothioate method of label attachment used for SLA and SLB is similar in its chemistry and its oligonucleotide end location to that used to label the $\psi_3$ RNA in our previous efforts[5] because study of end-labeled mini c TAR DNA followed shortly upon the $\psi_3$ RNA work. A 3-iodomethyl compound with a shorter tether to the nitroxide has more recently been used for making thio-ether end-labeled TAR RNA and will be used in the future for bilabel studies of both mini TAR RNA and mini c TAR DNA. Mini c TAR DNA with phosphorothioate modification was purchased from Trilink (TriLink Bio Technologies, San Diego, CA) or IDT (Integrated DNA Technologies, Inc., Skokie, IL). Spin-labels SLA and SLB, at the 5′ and 3′ termini, respectively, were attached by reacting iodo-spin-label precursors to phosphorothioate.[37] 3-(2-Iodoacetamide) proxyl (IPSL) and 3-iodomethyl-(1-oxy-2,2,5,5-tetramethylpyrroline) were purchased from Toronto Research Chemicals (North York, ON). Scheme 1 shows the thio-phosphorothioate methods of attaching spin-labels.

Labels SL1−SL3 in the loop, in the stem, and near the bulge of mini c TAR DNA, respectively, were attached by the reaction of a 4-isocyanoto TEMPO (Toronto Research Chemicals) spin-label precursor to a 2′-amino group on a cytidine sugar[14] to form a 2′-ureido−2′-amino linkage as shown in Scheme 2. Mini c TAR DNAs with specific 2′-amino groups in the loop


dx.doi.org/10.1021/bi301058q | *Biochemistry* 2012, 51, 8530−8541

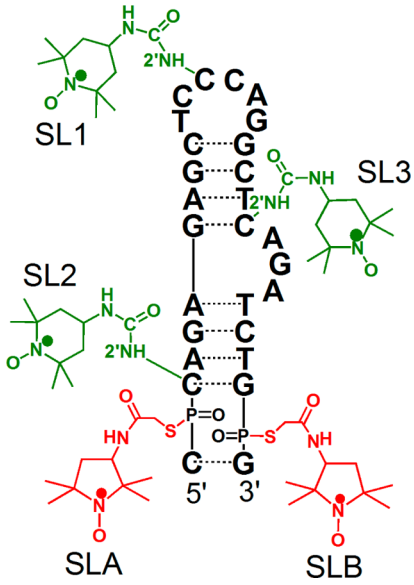


**Figure 2.** Positions of SLA, SLB, SL1, SL2, and SL3 that were the labeling sites on mini c TAR DNA. SLA and SLB, which are at the 5′ and 3′ termini, respectively, were attached by phosphorothioate linkages using iodo precursors. SL1−SL3, which are at cytidines of the loop, lower stem, and bulge region, respectively, were attached at a 2′-amino group on cytidine sugars via a ureido−2′-amino linkage.

(SL1), stem (SL2), or bulge (SL3) were obtained from TriLink Bio Technologies. The ureido linkage to the 2′-amino was chosen rather than a phosphorothioate linkage for our initial study of stem, loop, and bulge regions, because it was expected that the 2′-amino linkage would have less intrinsic mobility and would better report motion of the oligonucleotide to which it was tethered. For both the phosphorothioate and the 2′-amino methods of attachment, the detailed protocols for label attachment, for gel and HPLC purification, and for analysis of labeled product are provided in the Supporting Information (Figures 1S−3S). (Possible $R_p$ and $S_p$ diastereomers of phosphorothioate linkages[38] were not separated.)

**Scheme 2. Reaction of the 4-Isocyanato TEMPO Spin-Label with 2′-Aminocytidine To Form a Ureido−2′-Amino Linkage**

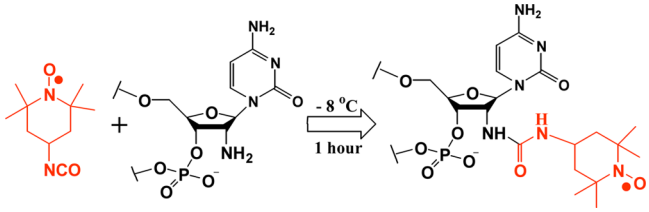


**Preparation of Nucleocapsid Protein NCp7.** NCp7 was prepared by solid phase peptide synthesis and with analysis methods similar to those described previously.[5,39−41] The final NCp7 concentration was determined by using an extinction coefficient ($\varepsilon_{280}$) of 6050 $M^{-1}$ $cm^{-1}$.[42]

**Nondenaturing Gel Shift Assays.** The interaction of NCp7 and mini c TAR DNA was monitored by nondenaturing gel assays as described previously for $\psi_3$ RNA,[5] and these are shown in Figure 4S of the Supporting Information to provide at various NCp7:c TAR DNA ratios a comparison of NCp7 binding to spin-labeled mini c DNA and NCp7 binding to unlabeled mini c TAR DNA. The spin-labeled and nonlabeled forms of mini c TAR DNA showed extremely similar NCp7 binding. The mini c TAR DNA by itself, either labeled or unlabeled, traveled fastest with unlabeled traveling slightly faster. At a ≥1:1 NCp7:mini c TAR DNA ratio, a low-molecular weight complex appeared, traveling slightly slower than the 30 bp marker that, in analogy with the findings on $\psi_3$ RNA, indicated a 1:1 complex. At higher ratios, more diffuse, more slowly moving, higher-molecular weight complexes appeared.

**Melting of Labeled and Unlabeled Mini c TAR DNA.** UV absorbance profiles at 260 nm, reflecting the hyperchromic increase caused by duplex melting, were obtained as a function of temperature in the range of 20−95 °C for both labeled and unlabeled mini c TAR DNA at a concentration of 2 μM. The melting profile was obtained by taking the first derivative of the

**Scheme 1. Reaction (a) of a Phosphorothioate Sulfur with 3-Iodomethyl-(1-oxy-2,2,5,5-tetramethylpyrroline) (blue) To Form a Phosphorothioate linkage and a Similar Reaction (b) with a 3-(2-Iodoacetamino) Proxyl Spin-Label (red)**

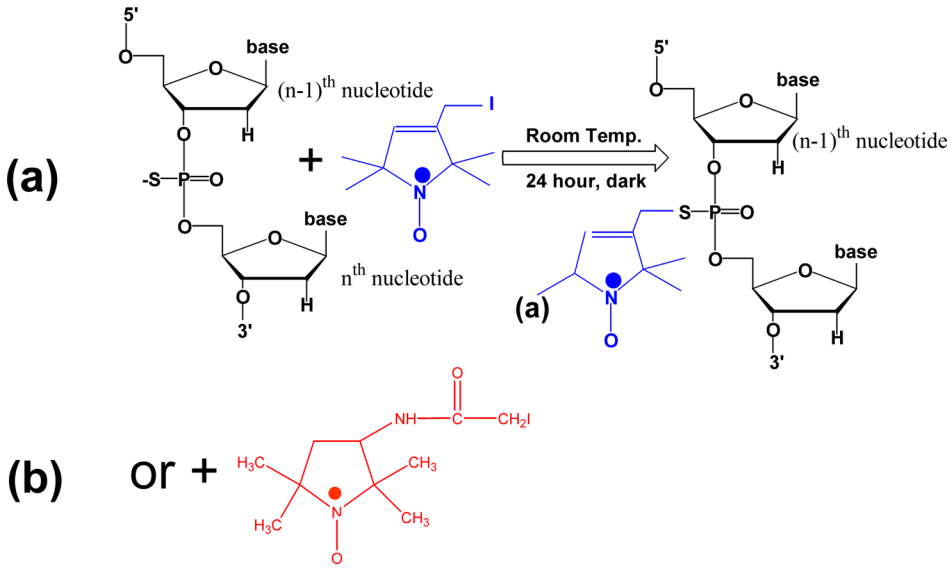



dx.doi.org/10.1021/bi301058q | Biochemistry 2012, 51, 8530−8541

absorbance with respect to temperature, and from these profiles, estimates were obtained by nonlinear least-squares parameter estimation of $T_m$ (melting temperature), $\Delta H$ (van't Hoff enthalpy), and $\Delta S$ (van't Hoff entropy) using a model that assumes a two-state sequential unfolding.[43] Melting temperatures of all mini c TAR DNAs, both labeled and unlabeled, were similar within 1 °C under the same solution conditions (Figure 5S of the Supporting Information), but the enthalpy of melting was diminished by labels in the bulge (SL3) and at the 5′ end (SL2) of mini c TAR DNA (Table 1S of the Supporting Information).

**EPR Spectroscopy.** *Apparatus.* At Albany, X-band (9.5 GHz) EPR spectra of spin-labeled mini c TAR DNA were recorded at room temperature using a high-sensitivity 9.5 GHz dielectric resonator that holds approximately 1 μL samples.[5,44−46] A microwave power of 0.64 mW and a modulation of ∼1 G were chosen so as not to broaden the EPR spectrum. For the 9.5 GHz study at ACERT, a Bruker ElexSys E500 spectrometer was used at room temperature (20 °C) and at 5 °C with a cavity resonator (SHQE4122). For the 9.5 GHz study at ACERT, samples of 1−1.5 μL were placed in a 0.50 cm (inside diameter) × 0.70 cm (outside diameter) quartz capillary with the end sealed by Dow Corning Silicon vacuum grease, and the spectrometer parameters were as follows: 1 G modulation amplitude, 100 kHz modulation frequency, 2 mW microwave power, and 100 G magnetic field sweep.

High-field EPR spectra were recorded on a state-of-the-art home-built spectrometer operating at 236.6 GHz[12] to study more explicitly the rapid probe motion. The field modulation was 9 G ptp. Quartz coverslips (ESCO, 12 mm diameter, ∼0.17 mm thickness) were used as the basis for double-stacked "sandwich" sample holders.[27,47] Approximately 2 μL of the sample was placed between a flat quartz coverslip and an etched quartz coverslip containing a circular well in the middle. The diameter of the well was ∼0.8 cm. A thin layer of vacuum grease was applied on the edges to seal the two coverslips. Two such samples were fixed together with vacuum grease to provide the sandwich samples containing ∼4.0 μL. The vertical distance between the centers of the two samples is one-half of a wavelength (0.63 mm). At 236.6 GHz, very low concentrations of the $Mn^{2+}$ contaminant can provide a background signal because the $Mn^{2+}$ line width is vastly sharpened at high frequency, because its width is inversely proportional to the square of the microwave frequency. This $Mn^{2+}$ signal is well understood, can be removed from spectra by computer methods, and, in fact, provides a field marker.

*EPR Line Shape Analysis for the Estimate of Tumbling Correlation Times via 9.5 GHz NLSL Analysis.* Random tumbling, as it modulates the anisotropic hyperfine and Zeeman interactions, causes the three hyperfine lines of the nitrogen $I$ = 1 $^{14}N$ nucleus of the nitroxide spin-label to vary differently in amplitude and line width. As the spin-label becomes less mobile, the outlying ($M = \pm 1$) peak heights diminish with respect to the central ($M = 0$) peak. This line width variation at 9.5 GHz is primarily due to the motional averaging of the nitrogen hyperfine interaction; 9.5 GHz EPR line shape simulations and correlation time determinations were based on the nonlinear least-squares limited stochastic Liouville (NLSL) fitting program developed by Freed and co-workers.[48] These simulations model the motion of the nitroxide by a rotational diffusion tensor, **R**. For our 9.5 GHz simulations, an isotropic tumbling diffusion rate [$R_{iso} = 1/(6\tau_{iso})$] generally sufficed, where $\tau_{iso}$ is the isotropic tumbling time (although an anisotropic rotation tensor was tried in a number of cases). For samples having slower tumbling caused by a 4:1 NCp7:mini c TAR DNA ratio, NLSL was used to estimate the percentage of slower and faster tumbling sites.

*Multifrequency SRLS Analysis.* Rapid subnanosecond dynamic modes, i.e., internal fluctuations, which may differ among the stem, loop, and bulge, were best resolved at higher frequencies. In contrast, nanosecond or longer global tumbling, large bending motions, and nanosecond conformational distortions would appear to be frozen at frequencies as high as 236.6 GHz but could affect the low-frequency (9.5 GHz) spectra. The high-frequency, high-field sensitivity to rapid tumbling motion is a consequence of the increased importance of the **g** tensor as the magnetic field is increased. The increased sensitivity to the **g** tensor allows high-frequency EPR to distinguish rapid rotations about the $g_x$, $g_y$, or $g_z$ tensor directions so that at high frequencies one can "read off" from the spectrum the nature of anisotropic motions.[12,49] An important aspect of the SRLS model is that the local reorientation of the spin-label may be restricted by a local potential and that order parameters, $S_{20}$ and $S_{22}$, reflecting axial and nonaxial contributions to the ordering, may be derived from this potential.

**Scheme 3. High-Frequency EPR Better Resolves Anisotropic Probe Motion**[a]

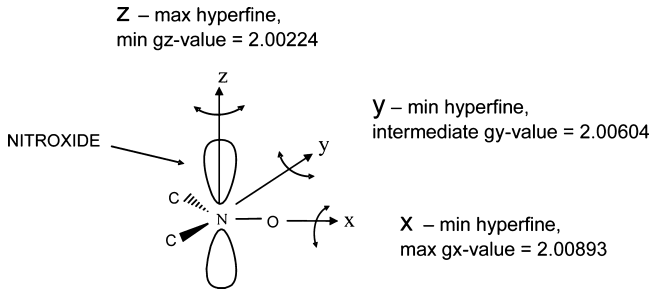


[a]It distinguishes $x$, $y$, or $z$ rotations because of its greater sensitivity to $g_x$, $g_y$, and $g_z$ anisotropy, respectively. Specifically for SL1−SL3, which have a TEMPO nitroxide, we take $g_x = 2.00893$, $g_y = 2.00604$, $g_z = 2.00224$, $A_x = 6.9$, $A_y = 7.6$, and $A_z = 36.5$ G.

*Pulse Dipolar Spectroscopy with Double Electron−Electron Resonance (DEER).* Using a 17.35 GHz home-built Ku-band pulse spectrometer,[50,51] DEER measurements were performed at 60 K. A four-pulse DEER sequence was applied with respective $\pi/2$, $\pi$, and $\pi$ pulse widths of 16, 32, and 32 ns, respectively, and a 32 ns $\pi$ pump pulse was used. The detection pulses were positioned at the low-field edge, and the pump pulse was positioned at the center of the nitroxide spin-label spectrum so that the frequency separation between detected and pumped pulses was 70 MHz. Distances measured were in the range of 2−5 nm, and the DEER evolution time period ($\tau_2$) was 1.6 μs, covering at least 2.5 periods of dipolar oscillations. The exponentially decaying background was removed from the raw time domain DEER signals. By application of the Tikhonov regularization (L-curve) method[36] and refinement by the maximum entropy method (MEM),[35] distances were reconstructed from the baseline-corrected and normalized signals.

## RESULTS

**Motion of Spin-Labeled Mini c TAR DNA Studied by High-Field, High-Frequency EPR.** Because of recent


dx.doi.org/10.1021/bi301058q | *Biochemistry* 2012, 51, 8530−8541

sensitivity advances [27] in high-frequency, high-field EPR, faster internal probe motion can be better understood. The spectra in Figure 3 provide a comparison of 9.5 and 236.6 GHz EPR spectra from mini c TAR DNA labeled at SL1, SL2, SL3, SLB, mini TAR RNA 3′ end labeled at SLB, and $\psi_3$ RNA labeled at its 5′ end.[a] The 9.5 GHz spectra, all having three fairly narrow lines, indicated an ostensibly isotropic tumbling with a correlation time on the order of 1 ns, like that of previously reported spin-labeled $\psi_3$ RNA.[5] However, there was a spectroscopic contrast at 236.6 GHz among the samples of mini c TAR DNA, mini TAR RNA, and $\psi_3$ RNA that were phosphorothioate end-labeled and the samples that were labeled by ureido−2′-amino linkages at SL1−SL3.[a] The contrast is due to differences in fast subnanosecond tumbling that is well sensed at 236.6 GHz, but not at 9.5 GHz. SL1−SL3 performed rapid, subnanosecond anisotropic motion about a preferential axis, which was at or near their nitroxide $g_x$ magnetic axis (see Scheme 3 for the definition of axes). The reorientation of the $g_x$ axis itself, with respect to the overall macromolecule, was considerably slower. The details of such anisotropic motions, in terms of a local rotation tensor and an ordering potential, are provided in Discussion. The end-labeled species of SLB mini c TAR DNA, SLB mini TAR RNA, and $\psi_3$ RNA all showed rapid isotropic tumbling that interchanged $x$, $y$, and $z$ axes in <1 ns.

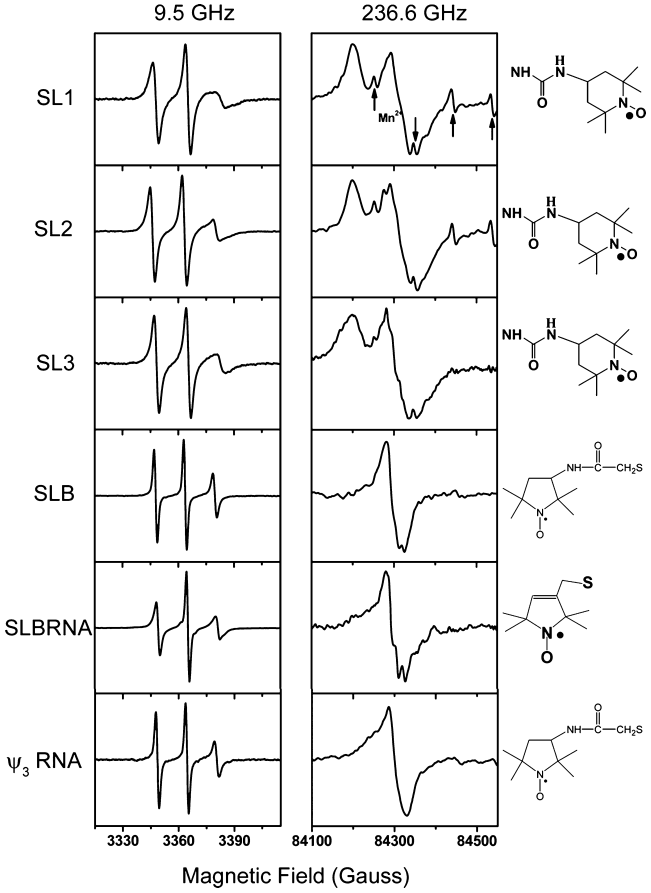


**Figure 3.** ESR spectra of mini c TAR DNA labeled at positions SL1, SL2, SL3, and SLB, mini TAR RNA labeled at its 3′ (SLB) terminus, and $\psi_3$ RNA labeled at its 5′ terminus. Concentrations of labels were approximately 100 $\mu$M (except that of SL3, which was 250 $\mu$M) in 20 mM Hepes (pH 7.5), 20 mM NaCl, and 0.2 mM $Mg^{2+}$ at 20 °C. The spectra are compared at EPR frequencies of 9.5 and 236.6 GHz to show the resolving power of high-frequency EPR for differences in motion. EPR conditions are given in Materials and Methods. The features labeled $Mn^{2+}$ are due to low-level $Mn^{2+}$ impurities whose line shapes are vastly sharpened at high frequencies and provide effective internal field markers.

There was a difference in the 236.6 GHz EPR line shape between the mini c TAR DNA and the two RNA derivatives, all labeled at or near the end of their stem. This difference, although marginally evident in the 20 °C spectra of Figure 3, was noteworthy at 5 °C as shown in Figure 4. The motion of the label on the mini TAR RNA slowed more than that of the corresponding label on the mini c TAR DNA and, by better resolution of its low-field $g_x$ shoulder, gave evidence of an increased anisotropy to its label motion at 5 °C. The label at the 5′ end of the $\psi_3$ RNA similarly slowed and showed evidence of anisotropic motion at lower temperatures. The thio-amido label was used for labeling the mini c TAR DNA and the $\psi_3$ RNA, and this label has potentially more flexible bonds between its phosphorothioate point of attachment and the nitroxide than does the thio-ether bond used for labeling the mini TAR RNA. However, see footnote *b*. Nevertheless, the label on the $\psi_3$ RNA, even though it is attached to the very end of the $\psi_3$ RNA oligonucleotide rather than between the final and penultimate nucleotides as in SLB mini c TAR DNA, showed less mobility and more anisotropy at 5 °C than did the same label on the mini c TAR DNA.

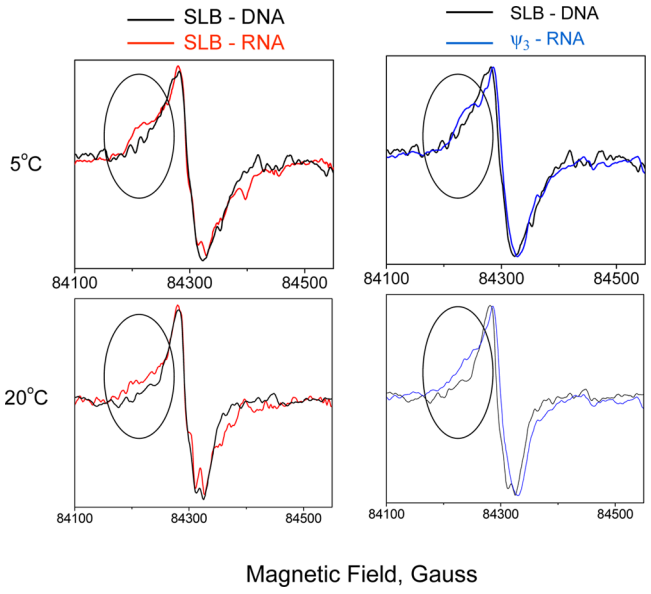


**Figure 4.** 236.6 GHz EPR spectra at 20 and 5 °C showing temperature-dependent differences in line shape that were observed for end-labeled SLB mini c TAR DNA, SLB mini TAR RNA, and $\psi_3$ RNA. The difference in the enclosed low-field region is largest at 5 °C. Besides the temperature, conditions for obtaining these spectra are as described in the legend of Figure 3.

**Motion of Spin-Labeled Mini c TAR DNA in the Presence of NCp7.** This section focuses on the dynamic changes due to added NCp7 as reported by spin-labels on mini c TAR DNA. Because 9.5 GHz EPR is sensitive to slower nanosecond tumbling times, these studies with NCp7 binding at a number of mini c TAR DNA:NCp7 ratios were undertaken with 9.5 GHz EPR.[c] The changes in the spin-label spectra upon addition of the first NCp7 and then the second NCp7 are shown in Figure 5A. In all cases, the tumbling of the spin-labels


dx.doi.org/10.1021/bi301058q | *Biochemistry* 2012, 51, 8530−8541

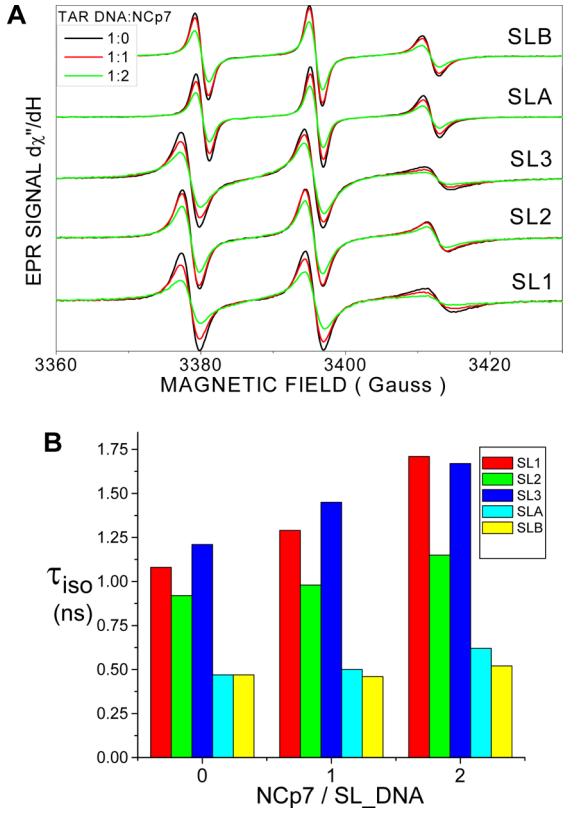


**Figure 5.** (A) 9.5 GHz EPR signals from mini c TAR DNA single spin-labels titrated with 0, 1, and 2 equiv of NCp7. The temperature was 20 °C, with a field modulation of 1.3 G. Spectra were normalized to the same number of spins by double integration. (B) Simplified isotropic correlation times ($\tau_{iso}$) of spin-labeled c TAR DNA species derived from the spectra in panel A by fitting spectra by the NLSL routine.[48,52]

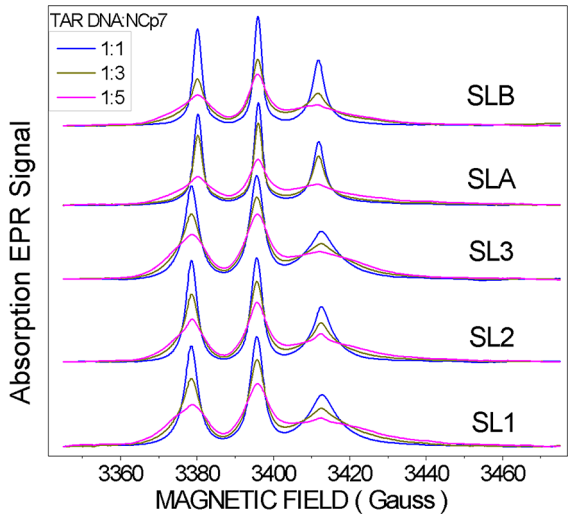


**Figure 6.** Comparison of the absorption 9.5 GHz EPR line shapes of the spin-labeled mini c TAR DNAs at low ionic strengths. The NCp7:mini c TAR DNA ratio was increased to ≥4, where a slowly tumbling complex forms. Spectra were normalized on the second integral. Sample conditions: 20 mM HEPES, 20 mM NaCl, 0.2 mM $MgCl_2$, pH 7.5, 20 °C. The mini c TAR DNA concentration was 100 $\mu$M.

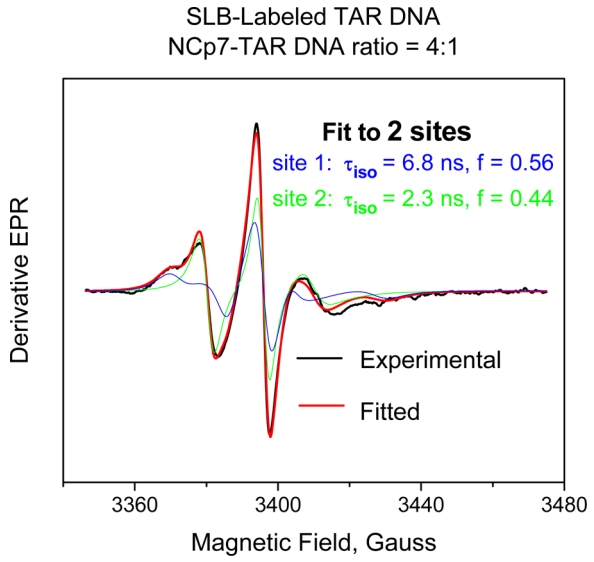


**Figure 7.** First-derivative 9.5 GHz EPR spectra obtained at room temperature from SLB-labeled mini c TAR DNA in the presence of a 4:1 NCp7:mini c TAR DNA molar ratio. The spectra show evidence of two differently immobilized species, one with a $\tau_{iso}$ of ~2.3 ns and the other with a $\tau_{iso}$ of ~6.8 ns.

was slowed by the NCp7, and different spin-label sites reported different sensitivities to NCp7. The probes at the loop (SL1) and bulge (SL3) were the slowest at the beginning and were most slowed by binding of NCp7. SL2 in the stem was faster and was less slowed by binding of NCp7. The simplified line shape analysis by a single isotropic correlation time, $\tau_{iso}$,[48,52] provided a semiempirical parameter for comparing differences in probe motion. Thus, a bar graph of $\tau_{iso}$ values is provided in Figure 5B, to show which probes were most impeded by addition of NCp7. Representative simulations used to obtain $\tau_{iso}$ from 9.5 GHz data are provided in Figure 6S of the Supporting Information.

When the NCp7:mini c TAR DNA ratio was increased to 4:1, there was a considerable slowing (tumbling time increased from ~1.0 to >5 ns) in the motion of the spin-label, where the broadening of the signals due to slowing of the tumbling is shown best by the integrated absorption EPR presentation in Figure 6. This phenomenon occurred for all the spin-labels studied and at a coverage of approximately seven nucleotides per NCp7, corresponding to four NCp7 molecules per mini c TAR DNA (noting that mini c TAR DNA is a 27-mer). The line shape broadening occurred at approximately the same NCp7 coverage where the previous study of $\psi_3$ RNA stem–loop structures[5] also showed considerable slowing. Interestingly, Figure 7 in the first-derivative mode indicates two differently mobile species for spin labeling site SLB under the condition where the NCp7:mini c TAR DNA molecular ratio is ≥4:1. As in the case of $\psi_3$ RNA, the immobilization in the presence of NCp7 coverage could be largely eliminated by increasing the ionic strength. We show representative 9.5 GHz EPR spectra in the presence of a 4:1 NCp7:mini c TAR DNA molecular ratio in Figure 7S of the Supporting Information, where there is progressive line shape narrowing as the NaCl concentration is increased from 20 mM to 150 mM to 400 mM.

**Changes to Mini c TAR DNA at a 4:1 NCp7:Mini c TAR DNA Molar Ratio.** The structure of the mini c TAR DNA within the slowly moving multi-NCp7 complexes provided a useful complement to the dynamic studies described above, especially because such complexes are not amenable to standard structural NMR and X-ray methods. For this reason,


dx.doi.org/10.1021/bi301058q | Biochemistry 2012, 51, 8530–8541

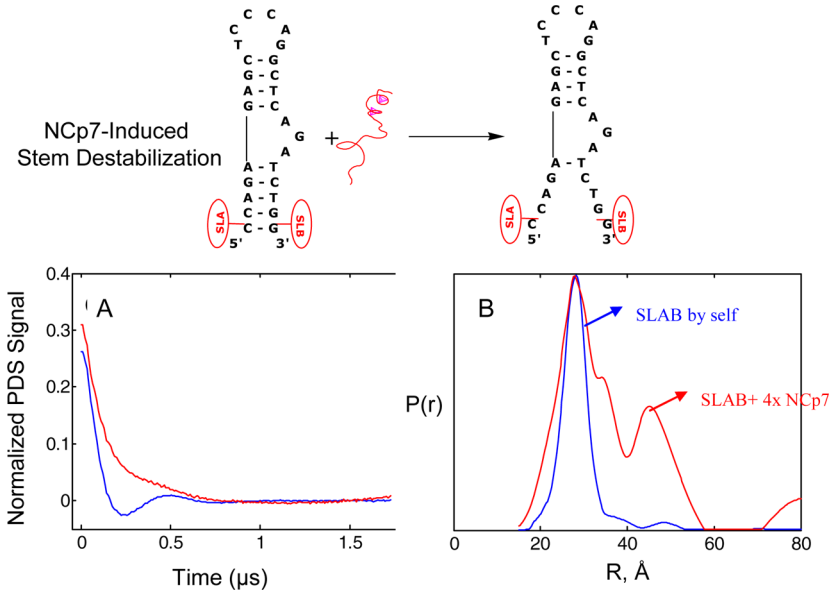


**Figure 8.** Doubly labeled mini c TAR DNA (blue) with NCp7 (red) at a 4:1 ratio. Structural evidence of fraying of ends of the stem–loop structure is obvious from PDS conducted at a 4:1 NCp7:bi-end-labeled mini c TAR DNA ratio and a low ionic strength. (A) Normalized PDS signals. (B) Comparison of the interprobe SLA–SLB distance distribution in the absence and presence of a 4:1 NCp7:bilabeled mini c TAR DNA ratio. The experimental spectrometer conditions are provided in Materials and Methods. Sample conditions: 20 mM HEPES, 20 mM NaCl, 0.2 mM $MgCl_2$, and pH 7.5. Samples were frozen in 10% glycerol to prevent tube breakage.

pulse dipolar spectroscopy (DEER) was performed on mini c TAR DNA that had been bilabeled at the SLA and SLB end positions by thio-amido labels. DEER spectra were taken both in the absence of NCp7 and in the presence of a 4:1 NCp7:mini c TAR DNA ratio. Figure 8 indicates the increased interprobe distance and the broadening of the distance distribution between bilabels SLA and SLB in the presence of a 4:1 NCp7:mini c TAR DNA ratio. There was still a large fraction of the mini c TAR DNA that approximately maintained the original SLA–SLB distance, while the remainder adopted a longer interprobe distance with greater breadth overall to its interprobe distribution.

## DISCUSSION

**Detailed Motion Inferred from Simultaneous SRLS Simulations of 9.5 and 236.6 GHz EPR Spectra.** In Figure 3, the effects of the motion of the probe, notably for SL1, SL2, and SL3 that have ureido–2′-amino spin-label linkages, are better resolved at high frequency. The spin-labels on mini c TAR DNA, mini TAR RNA, and $\psi_3$ RNA coupled by the more flexible phosphorothioate linkages at the end of the stem–loop structure showed isotropic tumbling at 236.6 GHz and 20 °C, but at 5 °C, the tumbling reported by the RNA samples showed incipient anisotropic motion about the $g_x$ axis, as indicated in Figure 4.

Because of the anisotropy of motion observed from their 236.6 GHz spectra, SL1, SL2, and SL3 were chosen for a comprehensive SRLS fit that included the local rapid diffusion tensor of the spin probe, a potential that in coupling the local rapid diffusion tensor to the global macromolecular tumbling led to an order tensor, and the global diffusion tensor of the entire mini c TAR DNA molecule. Such multiparameter, multifrequency simulations have been used to good effect to elucidate label motion for site-directed labels on proteins, notably in the study of T4 lysozyme.[27] This work is the first application of high-sensitivity, high-frequency EPR to spin-labeled oligonucleotides.

The combined 9.5 and 236.6 GHz spectra of SL1, SL2, and SL3 were simulated using the SRLS model program, in which $R_x$, $R_y$, $R_z$, $c_{20}$, and $R_c$ were varied as fitting parameters. $R_x$, $R_y$, and $R_z$ are the components of the anisotropic rotational diffusion tensor localized on the probe. The molecular rotational axis labels $x$, $y$, and $z$ are the same as those of the $g_x$, $g_y$, and $g_z$ axes, respectively (Scheme 3). $R_c$ is the diffusion coefficient for global tumbling. The dimensionless parameter $c_{20}$ refers to the axial restraining potential that couples local probe motion to overall global tumbling. $S_{20}$ is the order parameter associated with the potential parameter $c_{20}$; $S_{20}$ varies from zero, meaning no potential and hence no local ordering, to unity, meaning perfect alignment, i.e., zero flexibility. The $S_{20}$ value of $\approx$ 0.4 in Table 1 indicates behavior intermediate between these limits. The resultant parameters are listed in Table 1, and the spectra are overlaid with the resulting simulations in Figure 9. As shown in Table 1, $R_x \sim 3.3R_y \gg R_z$. This means that the $x$-axis and, to a lesser extent, the $y$-axis are the fast axes for the local motion of the probe. These local fast subnanosecond motions of $R_x$ and $R_y$ appear to be influenced by the local nucleotide environment, where SL2, located in a region of possible lower-stem duplex fraying, has the fastest local motion and where SL3, located near the bulge and near the upper duplex region, has the slowest local motion. SL1, in a nonduplex loop region, has local motion nearly as fast as that of SL2. The global tumbling rate, $R_c$, which is more than 1 order of magnitude slower than $R_x$ and $R_y$ should be affected by the tumbling of large, multinucleotide segments. Approximately, the probe performs rapid, but restricted (by the axial local potential), subnanosecond rotation about its $g_x$ axis, which is the axis pointing along the nitroxide NO bond, a direction that would also be the direction along bonds from the 2′-amino group to the nitroxide. The rapid restricted motion about this direction partially averages the hyperfine and magnetic Zeeman


dx.doi.org/10.1021/bi301058q | Biochemistry 2012, 51, 8530–8541

**Table 1. Simultaneous Fitting to the 9.5−236.6 GHz EPR Spectra of SL1, SL2, and SL3[a]**

| | SL1 | SL2 | SL3 |
|---|---|---|---|
| $R_c$ ($\times 10^7$ $s^{-1}$) | 2.6 ± 0.1 | 3.2 ± 0.1 | 3.3 ± 0.1 |
| $R_x$ ($\times 10^7$ $s^{-1}$) | 72.4 ± 6.5 | 75.3 ± 6.6 | 54.7 ± 4.9 |
| $R_y$ ($\times 10^7$ $s^{-1}$) | 19.2 ± 0.8 | 22.0 ± 0.9 | 19.5 ± 0.8 |
| $(R_x + R_y)/2$ ($\times 10^7$ $s^{-1}$) | 45.8 ± 3.3 | 48.9 ± 3.3 | 35.0 ± 2.5 |
| $R_z$ ($\times 10^7$ $s^{-1}$) | 0.6 ± 0.2 | 0.6 ± 0.2 | 1.5 ± 0.2 |
| $c_{20}$ | 1.86 ± 0.02 | 1.70 ± 0.02 | 1.67 ± 0.02 |
| $S_{20}$ | 0.41 | 0.38 | 0.37 |
| $W_{9.5}$ (G) | 0.94 | 0.89 | 0.90 |
| $W_{240}$ (G) | 1.3 | 4.4 | 7.8 |

[a] $R_x$, $R_y$, $R_z$, $c_{20}$, and $R_c$ are major fitting parameters. The parameters used are those listed here and in Table 2S of the Supporting Information. All parameters were varied in the fitting process except for the ones labeled "fixed" in Table 2S. No additional parameters were included to produce the values listed here or in Table 2S. $\beta_d$, the angle between the nitroxide magnetic tensor and the fast diffusion tensor, was not included; in fact, a $\beta_d$ of 30° was tried, and the fit was poorer. Errors in parameters were estimated by randomly starting the fitting process within ±10% of the parameter values in Table 1 (or Table 2S) and then recording the resultant variation in the fitted parameters.

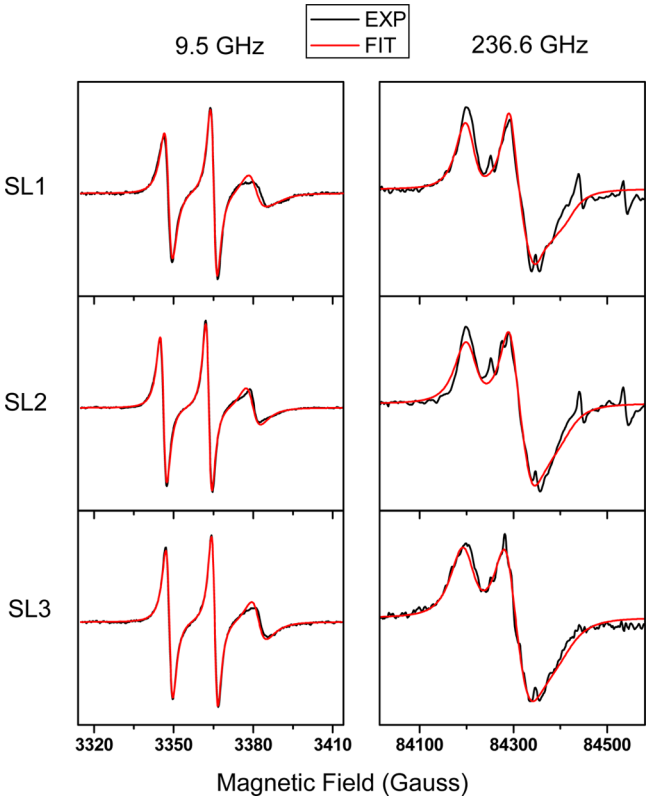


**Figure 9.** Combined simulations of 9.5 and 236.6 GHz spectra to provide evidence of the anisotropic diffusion tensor of the probe provided through the parameters for SL1, SL2, and SL3 in Table 1. $R_x$, $R_y$, $R_z$, $c_{20}$, and $R_c$ are the fitting parameters.

interactions corresponding to the *y*- and *z*-axes (Scheme 3). The slower restricted motion about the *y*-axis similarly partially averages *x* and *z* components, but less effectively especially given the much larger difference $[(g_x - g_z) \times 10^4 \sim 67$ vs $(g_x - g_y) \times 10^4 \sim 29]$ to be averaged by the motion. This ultimately means that the motion about the *z*-axis (which is not restricted by the axial potential) is very slow. On the other hand, the $g_x$ axis itself only slowly reorients so that low-field, $g_x$ features remain in the 236.6 GHz spectra of SL1, SL2, and SL3.

First, one notes that $R_c$ values are comparable for all three labels as they should be for the overall tumbling rate, but slow local effects could lead to small differences. Also, SL3 exhibits a slower $R_x$ but a faster $R_z$ than the other two. They all have a comparable local ordering, $S_{20}$. In general, one finds that $W_{240} > W_{9.5}$, where $W_{240}$ and $W_9$ are the residual (Lorentzian) widths at 240 and 9.5 GHz, respectively, that supplement the widths due to partial averaging of the magnetic tensors by the motions.[27] This could be due to local differences in solvent polarity and H-bonding,[27] differences in local conformations, and/or some aggregation from undissolved labeled TAR DNA. Because the SL3 concentration was 250 μM, whereas the SL1 and SL2 concentrations were 100 μM, this could be the explanation for the large $W_{240}$ for the former.

A second SRLS approach is provided in the Supporting Information (see Table 2S and Figure 8S), in which an axial local diffusion tensor was assumed, as opposed to the rhombic tensor used above, but a rhombic restraining potential was assumed for the second SRLS approach, as opposed to the axial restraining potential used above. The total number of fitting parameters was the same in these two methods of simulation, but the one in the Supporting Information was less stable, requiring fixing some of the parameters. For either method, the motion of the probe was faster for SL2 than for SL1 or SL3, and the fastest local tumbling motion was about the $g_x$ axis.

In Figure 4, a low-field 236.6 GHz EPR feature emerged at 5 °C from the mini TAR RNA labeled at the 3′ terminus and to a lesser extent from $\psi_3$ RNA labeled at the 5′ terminus. The emergence of this feature implied preferential slowing of the probe motion along the $g_x$ direction in the two RNA samples. Both the label with thio-ether attachment for the mini TAR RNA and that with the thio-amido attachment for $\psi_3$ RNA showed slower, anisotropic motion at 5 °C. The feature implying anisotropic motion was absent from the 3′ probe signal from mini c TAR DNA, for which the probe tumbling motion remained more isotropic and faster. The mini c TAR DNA versus TAR RNA difference would be consistent with preferential melting of the lower stem of mini c TAR DNA, which has been inferred from the absence of imino base pair proton features from the lower stem of mini c TAR DNA.[6] The thermodynamic information in Table 1S of the Supporting Information shows that the spin-label at position SLB of mini c TAR DNA had, in comparison with that of the unlabeled mini c TAR DNA, no perturbation to the melting temperature or the thermodynamic stability ($\Delta G$) at 37 or 20 °C, so it is not the label perturbation that is causing melting. The dynamic difference shown in Figure 4 between mini c TAR DNA and mini TAR RNA suggests future comprehensive dynamic comparisons of mini c TAR DNA and mini TAR RNA label motion at numerous corresponding positions, conceivably with pure $R_p$ and $S_p$ diastereomers[38] of the phosphorothioate linkages.[c]

**9.5 GHz Study of the NCp7-Related Change in Probe Mobility.** The spectroscopic differences between labels SL1, SL2, and SL3 (Figure 5A), with SL2 showing the most mobility and SL3 showing less mobility, imply less dynamic motion on the 1 ns time scale near the loop (SL1) and the bulge (SL3) than in the stem (SL2).[b,c] Although the time scale of motion was different, the high-frequency 236.6 GHz EPR findings were similar in that there was less rapid dynamic motion in the bulge (SL3). We recognize that the ureido−2′-amino attachment of


dx.doi.org/10.1021/bi301058q | *Biochemistry* 2012, 51, 8530−8541

the label decreased the enthalpy of melting for SL2 and SL3, where the labeling sites are in regions of base pairing. An explanation for this enthalpy change is that the ureido−2′-amino linkage, although not in the immediate vicinity of DNA bases, could disrupt sugar puckers and rotations so as to interfere with base pairing and stacking. The correlation times, $\tau_{iso}$ (Figure 5B), are lower than expected for the overall global tumbling time of mini c TAR DNA (taken as an approximate cylinder with a 20 Å diameter and a 40 Å length, leading to $\tau_{\perp}$ = 5.8 ns and $\tau_{\parallel}$ = 2.6 ns[53]), but still considerably slower than subnanosecond fast local probe motion observed via 236.6 GHz EPR. The nanosecond time scale of the motion would be the time for dynamic motion of a many-base segment of the mini c TAR DNA, but not of the entire molecule. The faster tumbling motion occurs in the lower stem (Figure 5B), suggested to be partially and dynamically melted even in the absence of NCp7.[6]

The labels in the loop and bulge show more sensitivity than the ones in the lower stem to the binding of NCp7, at 1:1 and 2:1 NCp7:mini c TAR DNA ratios. A previous NMR study of mini c TAR DNA complexed to 11−55 NCp7, lacking the basic tail of residues 1−10[11] and conducted at an ionic strength lower than that in our study, indicated a specific interaction of 11−55 NCp7 with unpaired bases in the guanidine region at the bottom of the mini c TAR DNA stem. The NCp7 that we use is 1−55 NCp7, containing both the zinc fingers that specifically recognize unpaired bases and a positively charged, basic tail of residues 1−10 that is thought to nonspecifically bind oligonucleotides. It seems less likely that binding of 1−55 NCp7 to the lower stem would perturb labels above the bulge (SL1 and SL3) than below (SL2). However, binding of NCp7 to the lower stem could in principle still diminish the conformational flexibility centered at the bulge and thereby indirectly diminish motion sensed by labels at the loop and bulge in the upper part of mini c TAR DNA. The implication of the slower NCp7-induced tumbling of SL1 and SL3 compared to that of SL2 is either that the position of binding for the 1−55 NCp7 complex is on the loop, bulge, and upper stem or that if there NCp7 binds to the lower stem, then immobilization and loss of conformational flexibility extend to the upper stem and loop.

The slower tumbling at a 2:1 NCp7:mini c TAR DNA ratio suggests that a second binding site for NCp7 impeded the motion, especially that of SL1 and SL3. Two binding sites have been implied by isothermal titration and gel binding studies.[11] It is possible that one or both of the NCp7 molecules that do bind are exchanging rapidly on the NMR time scale[11] but not the EPR time scale. Such exchange would impede motion on the EPR time scale but would not contribute well-defined structural features needed for NMR structural studies of TAR−NCp7 complexes.

**Properties of NCp7−Mini c TAR DNA Complexes Created at a 4:1 NCp7:Mini c TAR DNA Ratio.** Significant line shape broadening shown in Figure 6 occurred at a 4:1 NCp7:mini c DNA ratio, which is approximately one NCp7 per seven bases. This is the coverage at which annealing also occurs[3,4,31] and destabilization of the stem−loop structure has been proposed from FRET study.[32,33,54] The 9.5 GHz EPR spectra indicated considerable immobilization of the spin-label for all the locations studied. Similar behavior with a coverage of at least one NCp7 per seven oligonucleotide bases was noted in the previously reported study of $\psi_3$ RNA with NCp7.

Complexes with a coverage of one NCp7 per seven bases have been described as being "fuzzy" or molten globule-like complexes,[55] not amenable to NMR structural methods. A method for obtaining the underlying structure for such disordered systems is pulse dipolar EPR spectroscopy (PDS) of bilabels. The bilabels themselves are considerably smaller than FRET probes; they do not require potentially perturbing long tethers that remove them from the site of interest or separate donor and acceptor forms. In Figure 8, the evidence of NCp7-induced melting of the ends of c mini DNA is shown where both the 3′ and 5′ end have a spin-label. The ∼25 Å interprobe distance in the absence of NCp7 is due to the diameter of the duplex structure and the length of each tether. That distance is consistent with previously determined interprobe distances between two spin-labels attached to complementary, diametrically opposed phosphorothioates in the middle of a nonfrayed duplex DNA.[37,56,57] The implication is that in the absence of NCp7, the duplex structure in mini c TAR DNA below the bulge is not grossly frayed, even though its bases may undergo dynamic exchange of imino protons.[6] The presence of NCp7 at a 4:1 NCp7:mini c TAR DNA ratio clearly causes a sizable fraction of the mini c TAR DNA to come apart; the interprobe distance nearly doubles for that substantial fraction. Quantitative details of the interprobe distribution, not simply semiquantitative evidence of destabilization and fraying, are provided by the Tikhonov reconstruction of the interprobe distance distribution.[35,36] In the ambient-temperature 9.5 GHz EPR data of Figure 7 from a 4:1 NCp7:mini c DNA ratio, there was evidence of a fraction of species having slow >5 ns tumbling and another fraction having a tumbling time of ∼2 ns. The interlabel distance distribution of Figure 8 shows a fraction of more thoroughly frayed species having interprobe distances of >40 Å, and another less frayed fraction having interprobe distances closer to the unperturbed distance of 25 Å. It is unlikely that the fraction of bilabeled mini c TAR DNA in Figure 8, having an interprobe distance of ∼25 Å, is from mini c TAR DNA not at all bound to NCp7 because the typical constant for dissociation of NCp7 from oligonucleotides is less than micromolar,[11,58] because the ambient-temperature EPR of spin-labeled mini c TAR DNA in the presence of a 4-fold excess of NCp7 showed no evidence of rapidly moving, unbound mini c TAR DNA (Figure 7), and because the DEER feature with peak at 25 Å in the presence of NCp7 is broadened from destabilization by NCp7. These findings provide explicit physical evidence of the simultaneous existence of both the closed conformation and the partially open "Y" conformation of mini c TAR DNA. It is tempting to suggest that within the condensate having a 4:1 NCp7:mini c TAR DNA ratio the fraction of species with the slower spin dynamics ($\tau_{iso}$ > 5 ns) in Figure 7 is the thoroughly frayed fraction of mini c TAR DNA, while the species with more rapid spin dynamics ($\tau_{iso}$ ∼ 2 ns) is the less frayed.

## SUMMARY

In summary, ambient-temperature spin-label studies with 240 GHz EPR provided information about rapid subnanosecond, hindered, local anisotropic motions and showed differences in these motions, where the most rapid motion was in the lower stem. High-frequency EPR showed a dynamic difference between the end-labeled mini c TAR DNA and the mini TAR RNA and the $\psi_3$ RNA, implying a more ordering environment of the label at 5 °C in the two RNAs. These dynamic differences among stem, loop, and bulge and between mini c TAR DNA and mini TAR RNA provide insight into oligonucleotide dynamics, and they point to future comparative


dx.doi.org/10.1021/bi301058q | Biochemistry 2012, 51, 8530−8541

RNA−DNA studies.[c] The slowing of nanosecond tumbling motions of large segments of the oligonucleotide, which are best observed by 9.5 GHz EPR, was enhanced by increasing the nucleocapsid protein NCp7:mini c TAR DNA ratio from zero to one to two. A greater slowing was observed from the labels in the loop and near the bulge of mini c TAR DNA. This differential dynamic sensitivity to the binding of NCp7, as probed by EPR, is thus a functional aspect of mini c TAR. At a 4:1 NCp7:mini c TAR DNA ratio, there was significantly slowed tumbling of all labels, indicating, as seen previously with $\psi_3$ RNA,[5] the condensation of NCp7 with mini c TAR DNA. At a 4:1 NCp7:mini c TAR DNA ratio, concomitant structural evidence of partial melting and a broadened 3′−5′ end-to-end distance distribution of the mini c TAR DNA were obtained by pulse dipolar EPR spectroscopy (DEER) of bilabels attached near the 3′ and 5′ termini of the mini c TAR DNA.

## ■ ASSOCIATED CONTENT

### Supporting Information

Protocols for labeling phosphorothioate linkages, including Figure 1S that shows the HPLC purification trace for labeled mini c TAR DNA and Figure 2S that shows analytical gel traces for labeled mini c TAR DNA. Protocols for the preparation of spin-labeled mini c TAR DNA via the reaction of 2′-amino-2′-deoxycytidine and 4-isocyanato-2,2,6,6-tetramethylpiperidine 1-oxyl, including Figure 3S that shows analytical gel traces for mini c TAR DNA labeled by this method. Nondenaturing gel shift assays showing the similarity of labeled and unlabeled mini c TAR DNA binding to NCp7, including Figure 4S that shows the gel scans. Melting of labeled and unlabeled mini c TAR DNA as monitored by UV−vis temperature melts at 260 nm, including Figure 5S that shows the melting profiles ($\delta A/\delta T$ at 260 nm) for wild-type and labeled mini c TAR DNA and Table 1S that provides thermodynamic parameters $\Delta H$, $\Delta S$, $\Delta G$, and $T_m$. Figure 6S comparing simulated 9.5 GHz EPR spectra from SL1, SL2, SL3, SLA, and SLB to experimental spectra obtained in the presence of a 2-fold excess of NCp7. Figure 7S showing the effect of changing the ionic strength on the breadth of the 9.5 GHz EPR spectrum of spin-labeled mini c TAR DNA in the presence of a 4:1 NCp7:mini c TAR DNA ratio. Simulations of the motion of spin-labeled mini c TAR DNA as studied by high-field, high-frequency EPR, where axial symmetry is assumed for the local probe diffusion tensor, including Figure 8S that shows SRLS simulations and Table 2S that lists the resultant EPR fitting parameters. This material is available free of charge via the Internet at http://pubs.acs.org.

## ■ AUTHOR INFORMATION


### Corresponding Author

*Telephone: (518) 442-4551. Fax: (518) 442-3462. E-mail: cps14@albany.edu.

### Present Addresses

[‖]State Key Laboratory of Magnetic Resonance and Atomic and Molecular Physics, Wuhan Institute of Physics and Mathematics, Chinese Academy of Sciences, Wuhan, Hubei 430071, China.

[⊥]Department of Chemistry, University of California, One Shields Avenue, Davis, CA 95616.



### Funding

This work was supported by the National Institutes of Health (GM066253-01A1 and 3RO1GM06625304S1 to C.P.S., National Center for Research Resources Grant P41RR016292, and National Institute of General Medical Sciences Grant P41GM103521 to J.H.F.) and an RNA Institute Interdisciplinary Pilot Research Program 2010 Award, UAlbany, to K.A.E.

### Notes

The authors declare no competing financial interest.


## ■ ACKNOWLEDGMENTS


We are grateful to Prof. Carla Theimer (Department of Chemistry, University at Albany) for providing lab space and technical advice for the preparation and characterization of oligonucleotides. We thank Dr. Peter P. Borbat (Department of Chemistry and Chemical Biology and ACERT, Cornell University) for taking and analyzing the pulse dipolar EPR spectra.


## ■ ABBREVIATIONS

EPR, electron paramagnetic resonance; SRLS, slowly relaxing local structure; NLSL, nonlinear least-squares limited; DEER, double electron−electron resonance; PDS, pulse dipolar spectroscopy.

## ■ ADDITIONAL NOTES

[a]Labeling of a phosphorothioate group by an iodo spin-label precursor was done on SLB mini TAR DNA, SLB mini TAR RNA, and $\psi_3$ RNA. For the SLB mini c TAR DNA, a phosphorothioate between the 3′ G and its neighboring G was labeled with an iodoacetamide spin-label precursor. For the SLB mini TAR RNA, a phosphorothioate between the 3′ G and its neighboring G was labeled with an iodomethyl spin-label precursor. For the $\psi_3$ RNA, a phosphorothioate at the terminal 5′ G was labeled with an iodoacetamide spin-label precursor.

[b]Work in progress at X-band with thio-ether label linkages in the corresponding loop, stem, and bulge near the positions of previous ureido−2′-amino labeling sites SL1, SL2, and SL3 has shown the same order of mobility as SL1, SL2, and SL3 did, although the motion of the thio-ether labels is overall faster than that of the ureido labels. A related study with thio-ether linkages at corresponding loop, stem, and bulge positions is underway to compare motions of mini c TAR DNA and mini TAR RNA. For our future experimental design, we are grateful to a reviewer for suggesting looking for $R_p$ versus $S_p$ diastereomeric differences in the phosphorothioate labeling site between mini c TAR DNA and mini TAR RNA.

[c]To assess the utility of high-field EPR to studies of oligonucleotides, our initial high-field study was limited to spin-labeled mini c TAR DNA and mini TAR RNA oligonucleotides by themselves in the absence of NCp7. In synchrony with technical improvements to high-field EPR for aqueous samples, additional high-frequency EPR directed at NCp7 complexes of mini TAR is underway.

## ■ REFERENCES


(1) Johnson, P. E., Turner, R. B., Wu, Z. R., Hairston, L., Guo, J., Levin, J. G., and Summers, M. F. (2000) A mechanism for plus-strand transfer enhancement by the HIV-1 nucleocapsid protein during reverse transcription. *Biochemistry 39*, 9084−9091.

(2) Guo, J., Henderson, L. E., Bess, J., Kane, B., and Levin, J. G. (1997) Human immunodeficiency virus type 1 nucleocapsid protein promotes efficient strand transfer and specific viral DNA synthesis by inhibiting TAR-dependent self-priming from minus-strand strong-stop DNA. *J. Virol. 71*, 5178−5188.

(3) Vo, M. N., Barany, G., Rouzina, I., and Musier-Forsyth, K. (2009) HIV-1 nucleocapsid protein switches the pathway of transactivation

response element RNA/DNA annealing from loop-loop "kissing" to "zipper". *J. Mol. Biol. 386*, 789−801.
(4) Vo, M. N., Barany, G., Rouzina, I., and Musier-Forsyth, K. (2006) Mechanistic studies of mini-TAR RNA/DNA annealing in the absence and presence of HIV-1 nucleocapsid protein. *J. Mol. Biol. 363*, 244−261.
(5) Xi, X., Sun, Y., Karim, C. B., Grigoryants, V. M., and Scholes, C. P. (2008) HIV-1 nucleocapsid protein NCp7 and its RNA stem loop 3 partner: Rotational dynamics of spin-labeled RNA stem loop 3. *Biochemistry 47*, 10099−10110.
(6) Zargarian, L., Kanevsky, I., Bazzi, A., Boynard, J., Chaminade, F., Fosse, P., and Mauffret, O. (2009) Structural and dynamic characterization of the upper part of the HIV-1 cTAR DNA hairpin. *Nucleic Acids Res. 37*, 4043−4054.
(7) Zhang, Q., Sun, X., Watt, E. D., and Al-Hashimi, H. M. (2006) Resolving the motional modes that code for RNA adaptation. *Science 311*, 653−656.
(8) Zhang, Q., Stelzer, A. C., Fisher, C. K., and Al-Hashimi, H. M. (2007) Visualizing spatially correlated dynamics that directs RNA conformational transitions. *Nature 450*, 1263−1267.
(9) Getz, M., Sun, X., Casiano-Negroni, A., Zhang, Q., and Al-Hashimi, H. M. (2007) NMR studies of RNA dynamics and structural plasticity using NMR residual dipolar couplings. *Biopolymers 86*, 384−402.
(10) Sun, X., Zhang, Q., and Al-Hashimi, H. M. (2007) Resolving fast and slow motions in the internal loop containing stem-loop 1 of HIV-1 that are modulated by $Mg^{2+}$ binding: Role in the kissing-duplex structural transition. *Nucleic Acids Res. 35*, 1698−1713.
(11) Bazzi, A., Zargarian, L., Chaminade, F., Boudier, C., De Rocquigny, H., Rene, B., Mély, Y., Fosse, P., and Mauffret, O. (2011) Structural insights into the cTAR DNA recognition by the HIV-1 nucleocapsid protein: Role of sugar deoxyriboses in the binding polarity of NC. *Nucleic Acids Res. 39*, 3903−3916.
(12) Earle, K. A., Dzikovski, B., Hofbauer, W., Moscicki, J. K., and Freed, J. H. (2005) High-frequency ESR at ACERT. *Magn. Reson. Chem. 43* (Spec no.), S256−S266.
(13) Qin, P. Z., Butcher, S. E., Feigon, J., and Hubbell, W. L. (2001) Quantitative analysis of the isolated GAAA tetraloop/receptor interaction in solution: A site-directed spin labeling study. *Biochemistry 40*, 6929−6936.
(14) Edwards, T. E., Okonogi, T. M., Robinson, B. H., and Sigurdsson, S. T. (2001) Site-specific incorporation of nitroxide spin-labels into internal sites of the TAR RNA; structure-dependent dynamics of RNA by EPR spectroscopy. *J. Am. Chem. Soc. 123*, 1527−1528.
(15) Edwards, T. E., Okonogi, T. M., and Sigurdsson, S. T. (2002) Investigation of RNA-protein and RNA-metal ion interactions by electron paramagnetic resonance spectroscopy. The HIV TAR-Tat motif. *Chem. Biol. 9*, 699−706.
(16) Edwards, T. E., and Sigurdsson, S. T. (2002) Electron paramagnetic resonance dynamic signatures of TAR RNA-small molecule complexes provide insight into RNA structure and recognition. *Biochemistry 41*, 14843−14847.
(17) Qin, P. Z., Hideg, K., Feigon, J., and Hubbell, W. L. (2003) Monitoring RNA base structure and dynamics using site-directed spin labeling. *Biochemistry 42*, 6772−6783.
(18) Edwards, T. E., Robinson, B. H., and Sigurdsson, S. T. (2005) Identification of amino acids that promote specific and rigid TAR RNA-tat protein complex formation. *Chem. Biol. 12*, 329−337.
(19) Popova, A. M., Kalai, T., Hideg, K., and Qin, P. Z. (2009) Site-specific DNA structural and dynamic features revealed by nucleotide-independent nitroxide probes. *Biochemistry 48*, 8540−8550.
(20) Grant, G. P., Boyd, N., Herschlag, D., and Qin, P. Z. (2009) Motions of the substrate recognition duplex in a group I intron assessed by site-directed spin labeling. *J. Am. Chem. Soc. 131*, 3136−3137.
(21) Earle, K. A., and Freed, J. H. (1999) Quasioptical hardware for a flexible FIR-EPR spectrometer. *Appl. Magn. Reson. 16*, 247−272.
(22) Freed, J. H. (2000) New technologies in electron spin resonance. *Annu. Rev. Phys. Chem. 51*, 655−689.
(23) Borbat, P. P., Costa-Filho, A. J., Earle, K. A., Moscicki, J. K., and Freed, J. H. (2001) Electron spin resonance in studies of membranes and proteins. *Science 291*, 266−269.
(24) Bennati, M., and Prisner, T. F. (2005) New Developments in High Field Electron Paramagnetic Resonance with Applications in Structural Biology. *Rep. Prog. Phys. 68*, 411.
(25) Liang, Z., and Freed, J. H. (1999) An assessment of the applicability of multifrequency ESR to study the complex dynamics of biomolecules. *J. Phys. Chem. B 103*, 6384−6396.
(26) Polimeno, A., and Freed, J. H. (1995) Slow motional ESR in complex fluids: The slowly relaxing local structure model of solvent cage effects. *J. Phys. Chem. 99*, 10995−11006.
(27) Zhang, Z., Fleissner, M. R., Tipikin, D. S., Liang, Z., Moscicki, J. K., Earle, K. A., Hubbell, W. L., and Freed, J. H. (2010) Multifrequency electron spin resonance study of the dynamics of spin labeled T4 lysozyme. *J. Phys. Chem. B 114*, 5503−5521.
(28) Pitt, S. W., Zhang, Q., Patel, D. J., and Al-Hashimi, H. M. (2005) Evidence that electrostatic interactions dictate the ligand-induced arrest of RNA global flexibility. *Angew. Chem., Int. Ed. 44*, 3412−3415.
(29) Fisher, C. K., Zhang, Q., Stelzer, A., and Al-Hashimi, H. M. (2008) Ultrahigh resolution characterization of domain motions and correlations by multialignment and multireference residual dipolar coupling NMR. *J. Phys. Chem. B 112*, 16815−16822.
(30) Zhang, Q., and Al-Hashimi, H. M. (2009) Domain-elongation NMR spectroscopy yields new insights into RNA dynamics and adaptive recognition. *RNA 15*, 1941−1948.
(31) Vo, M. N., Barany, G., Rouzina, I., and Musier-Forsyth, K. (2009) Effect of $Mg^{2+}$ and $Na^{+}$ on the nucleic acid chaperone activity of HIV-1 nucleocapsid protein: Implications for reverse transcription. *J. Mol. Biol. 386*, 773−788.
(32) Hong, M. K., Harbron, E. J., O'Connor, D. B., Guo, J., Barbara, P. F., Levin, J. G., and Musier-Forsyth, K. (2003) Nucleic acid conformational changes essential for HIV-1 nucleocapsid protein-mediated inhibition of self-priming in minus-strand transfer. *J. Mol. Biol. 325*, 1−10.
(33) Cosa, G., Harbron, E. J., Zeng, Y., Liu, H. W., O'Connor, D. B., Eta-Hosokawa, C., Musier-Forsyth, K., and Barbara, P. F. (2004) Secondary structure and secondary structure dynamics of DNA hairpins complexed with HIV-1 NC protein. *Biophys. J. 87*, 2759−2767.
(34) Cosa, G., Zeng, Y., Liu, H. W., Landes, C. F., Makarov, D. E., Musier-Forsyth, K., and Barbara, P. F. (2006) Evidence for non-two-state kinetics in the nucleocapsid protein chaperoned opening of DNA hairpins. *J. Phys. Chem. B 110*, 2419−2426.
(35) Chiang, Y. W., Borbat, P. P., and Freed, J. H. (2005) Maximum entropy: A complement to Tikhonov regularization for determination of pair distance distributions by pulsed ESR. *J. Magn. Reson. 177*, 184−196.
(36) Chiang, Y. W., Borbat, P. P., and Freed, J. H. (2005) The determination of pair distance distributions by pulsed ESR using Tikhonov regularization. *J. Magn. Reson. 172*, 279−295.
(37) Cai, Q., Kusnetzow, A. K., Hubbell, W. L., Haworth, I. S., Gacho, G. P., Van Eps, N., Hideg, K., Chambers, E. J., and Qin, P. Z. (2006) Site-directed spin labeling measurements of nanometer distances in nucleic acids using a sequence-independent nitroxide probe. *Nucleic Acids Res. 34*, 4722−4730.
(38) Grant, G. P., Popova, A., and Qin, P. Z. (2008) Diastereomer characterizations of nitroxide-labeled nucleic acids. *Biochem. Biophys. Res. Commun. 371*, 451−455.
(39) Zhang, Z., Xi, X., Scholes, C. P., and Karim, C. B. (2008) Rotational dynamics of HIV-1 nucleocapsid protein NCp7 as probed by a spin label attached by peptide synthesis. *Biopolymers 89*, 1125−1135.
(40) Karim, C. B., Kirby, T. L., Zhang, Z., Nesmelov, Y., and Thomas, D. D. (2004) Phospholamban structural dynamics in lipid bilayers probed by a spin label rigidly coupled to the peptide backbone. *Proc. Natl. Acad. Sci. U.S.A. 101*, 14437−14442.

(41) Karim, C. B., Zhang, Z., and Thomas, D. D. (2007) Synthesis of TOAC spin-labeled proteins and reconstitution in lipid membranes. *Nat. Protoc. 2*, 42−49.
(42) Tummino, P. J., Scholten, J. D., Harvey, P. J., Holler, T. P., Maloney, L., Gogliotti, R., Domagala, J., and Hupe, D. (1996) The in vitro ejection of zinc from human immunodeficiency virus (HIV) type 1 nucleocapsid protein by disulfide benzamides with cellular anti-HIV activity. *Proc. Natl. Acad. Sci. U.S.A. 93*, 969−973.
(43) Theimer, C. A., Wang, Y., Hoffman, D. W., Krisch, H. M., and Giedroc, D. P. (1998) Non-nearest neighbor effects on the thermodynamics of unfolding of a model mRNA pseudoknot. *J. Mol. Biol. 279*, 545−564.
(44) DeWeerd, K., Grigoryants, V., Sun, Y., Fetrow, J. S., and Scholes, C. P. (2001) EPR-detected folding kinetics of externally located cysteine-directed spin-labeled mutants of iso-1-cytochrome c. *Biochemistry 40*, 15846−15855.
(45) Grigoryants, V. M., and Scholes, C. P. (2006) Variable Velocity Liquid Flow EPR and Submillisecond Protein Folding (Chapter 5.3). In *Protein Structures: Methods in Protein Structure and Stability Analysis* (Uversky, V. N., and Permyakov, E. A., Eds.) pp 47−71, Nova Science Publishers, Inc., New York.
(46) Grigoryants, V. M., Veselov, A. V., and Scholes, C. P. (2000) Variable velocity liquid flow EPR applied to submillisecond protein folding. *Biophys. J. 78*, 2702−2708.
(47) Barnes, J. P., and Freed, J. H. (1997) Aqueous Sample Holders for High Frequency Electron Spin Resonance. *Rev. Sci. Instrum. 68*, 2838−2846.
(48) Budil, D. E., Lee, S., Saxena, S., and Freed, J. H. (1996) Nonlinear-Least-Squares Analysis of Slow-Motion EPR Spectra in One and Two Dimensions Using a Modified Levenberg-Marquardt Algorithm. *J. Magn. Reson., Ser. A 120*, 155−189.
(49) Dzikovski, B., Earle, K., Pachtchenko, S., and Freed, J. (2006) High-field ESR on aligned membranes: A simple method to record spectra from different membrane orientations in the magnetic field. *J. Magn. Reson. 179*, 273−279.
(50) Borbat, P. P., Crepeau, R. H., and Freed, J. H. (1997) Multifrequency two-dimensional Fourier transform ESR: An X/Ku-band spectrometer. *J. Magn. Reson. 127*, 155−167.
(51) Borbat, P. P., and Freed, J. H. (2007) Measuring distances by pulsed dipolar ESR spectroscopy: Spin-labeled histidine kinases. *Methods Enzymol. 423*, 52−116.
(52) Earle, K. A., and Budil, D. E. (2006) Calculating Slow-motion ESR Spectra of Spin-Labeled Polymers. In *Advanced ESR Methods in Polymer Research* (Schlick, S., Ed.) Chapter 3, John Wiley and Sons, New York.
(53) Tirado, M. M., and de la Torre, J. G. (1980) Rotational dynamics of rigid symmetric top macromolecules. Application to circular cylinders. *J. Chem. Phys. 73*, 1986−1993.
(54) Liu, H. W., Zeng, Y., Landes, C. F., Kim, Y. J., Zhu, Y., Ma, X., Vo, M. N., Musier-Forsyth, K., and Barbara, P. F. (2007) Insights on the role of nucleic acid/protein interactions in chaperoned nucleic acid rearrangements of HIV-1 reverse transcription. *Proc. Natl. Acad. Sci. U.S.A. 104*, 5261−5267.
(55) Darlix, J. L., Godet, J., Ivanyi-Nagy, R., Fosse, P., Mauffret, O., and Mély, Y. (2011) Flexible nature and specific functions of the HIV-1 nucleocapsid protein. *J. Mol. Biol. 410*, 565−581.
(56) Cai, Q., Kusnetzow, A. K., Hideg, K., Price, E., Haworth, I. S., and Qin, P. Z. (2007) Nanometer distance measurements in RNA using site-directed spin labeling. *Biophys. J. 93*, 2110−2117.
(57) Price, E. A., Sutch, B. T., Cai, Q., Qin, P. Z., and Haworth, I. S. (2007) Computation of nitroxide-nitroxide distances in spin-labeled DNA duplexes. *Biopolymers 87*, 40−50.
(58) Avilov, S. V., Godet, J., Piemont, E., and Mély, Y. (2009) Site-specific characterization of HIV-1 nucleocapsid protein binding to oligonucleotides with two binding sites. *Biochemistry 48*, 2422−2430.